Molecular Catalysis 449 (2018) 38–48

Contents lists available at ScienceDirect

Molecular Catalysis

journal homepage: www.elsevier.com/locate/mcat

Insight into the formation mechanism and kinetics for the oxidative carbonylation of methanol to dimethyl carbonate over CuO catalyst: Effects of Cu valence state and solvent environment

Li Kang[a], Jin Zhang[a], Riguang Zhang[a,b,*], Lixia Ling[a], Baojun Wang[a]

[a] Key Laboratory of Coal Science and Technology of Ministry of Education and Shanxi Province, Taiyuan University of Technology, Taiyuan 030024, Shanxi, China
[b] Department of Chemical Engineering and Department of Petroleum Engineering, University of Wyoming, Laramie, WY 82071, USA

ARTICLE INFO

Keywords:
Dimethyl carbonate
Oxidative carbonylation
Cu valence state
Solvent effect
Density functional theory

ABSTRACT

The formation mechanism and kinetics of dimethyl carbonate (DMC) via the oxidative carbonylation of methanol over Cu(II) catalyst have been investigated using density functional theory calculations under gas phase and solvent conditions. The results show that the preferred pathway of DMC formation in the gas phase is that via CO insertion into $(CH_3O)_2$ species, which is more favorable in kinetics than that via CO insertion into CH_3O; the rate-limiting step of DMC formation is CO insertion into $(CH_3O)_2$. Meanwhile, the kinetic results of DMC formation in the liquid phase show that the solvent can improve the catalytic activity of Cu(II) catalyst towards DMC formation in a liquid-phase slurry, especially in water. Moreover, the comparisons among different valence state Cu catalysts for the most favorable pathway of DMC formation indicate that Cu valence state has a significant effect on the formation mechanism of DMC. The calculated results can provide a clue to finely tune the catalytic activity of DMC formation over Cu-based catalyst using the valence state and solvent environments under the realistic conditions.

1. Introduction

Dimethyl carbonate (DMC) has been considered as a green chemical due to its high oxygen content, high dielectric constant, high solvency power, low viscosity and mild toxic [1–3]. For the synthesis of DMC, the various methods, the phosgenation of methanol, transesterification of urea, transesterification of EC and methanol, direct synthesis, oxidative carbonylation of methanol and so on, are proposed [4–10]. Among them, the oxidative carbonylation of methanol has been developed [11–22]; moreover, compared to other methods, the raw materials for the oxidative carbonylation of methanol are easily obtained from coal and natural gas [12,17,23,24]; further, the oxidative carbonylation of methanol is a thermodynamically favorable reaction [11,21,23], both the gas-phase [18,24–27] and liquid-phase methods [15,20] exist.

Up to now, the oxidative carbonylation of methanol is mainly carried out over CuCl catalyst. However, CuCl easily leads to the equipment corrosion and the catalyst deactivation due to Cl^- loss. Consequently, King et al. [19] discovered that chlorine was not necessary for Cu to catalyze the oxidative carbonylation of methanol. Thus, in order to avoid these problems, the free-chlorine Cu catalysts have been widely used, especially, Cu-exchanged zeolites is considered as one of the most potential catalysts [21,22,25,26,28–34], King [33] found that CuY zeolite exhibits good activity and selectivity for DMC formation without catalyst deactivation; moreover, Cu^+ ions are postulated to be the active species. Meanwhile, the mechanism for the oxidative carbonylation of methanol to DMC over Cu^+ species has been illustrated [11,22,31–34], for example, density functional theory (DFT) studies by Zheng and Bell [11] found that the molecularly adsorbed CH_3OH is oxidized by oxygen to either mono-methoxide or dimethoxide species; then DMC is formed from two distinct pathways: one is CO insertion into mono-methoxide to CH_3OCO, followed by its interaction with CH_3O to DMC; the other is CO insertion into dimethoxide to DMC. In addition, the mechanism and kinetics of oxidative carbonylation of methanol are also investigated employing DFT calculations over Cu_2O [31], $CuCl_2$–$PdCl_2$ bimetallic catalyst [35] and Cu(I)/β catalysts [36].

On the other hand, Wang et al. [16] prepared CuO–La_2O_3/activate carbon (AC) catalyst, which contained CuO and Cu_2O to provide Cu^+ and Cu^{2+} simultaneously; the results show CuO/Cu_2O could improve the stability and activity of the catalyst. Zhang et al. [37] found that CuO/AC performs a good catalytic activity for the oxidative carbonylation of methanol. Wang et al. [38] found that $PdCl_2$-$CuCl_2$ catalysts are more favorable than the single metal chloride catalysts. Tomishige et al. [39] suggested that $CuCl_2$/AC catalyst can promote the selectivity and activity of DMC formation through Cu-Cl-OH compounds. Sato

* Corresponding author at: No. 79 Yingze West Street, Taiyuan, 030024, China.
E-mail address: zhangriguang@tyut.edu.cn (R. Zhang).

https://doi.org/10.1016/j.mcat.2018.02.005
Received 24 November 2017; Received in revised form 1 February 2018; Accepted 9 February 2018

et al. [40] showed that Cu(II)-polymer complexes exhibits considerable catalytic activity and stability for DMC synthesis. Unfortunately, up to now, to the best of our knowledge, the detailed mechanism for the oxidative carbonylation of methanol to DMC over Cu(II) catalyst is still unclear, and therefore the effects of Cu valence state on the reaction mechanism and kinetics are also unknown.

Further, the reaction environments might change the chemical characteristics and reaction kinetics, in which the solvent environment plays an important role [41–47]. When the liquid-phase method is used for the oxidative carbonylation of methanol in liquid phase slurry, the chemical characteristics of catalyst and its catalytic performance may be different from those in the gas-phase method. Yet, a detailed understanding about the effects of solvent environments on the mechanism and kinetics of DMC formation is seldom considered.

This study was designed to understand the mechanism and kinetics for the oxidative carbonylation of methanol to DMC over Cu(II) catalyst, as well as the effects of Cu valence state and solvent environment. Here, the results are obtained by DFT calculations with the periodic slab model. Firstly, the mechanism and kinetics of DMC formation is examined over CuO catalyst, which is used to model Cu(II) catalyst. Then, the kinetic results of DMC formation in gas phase are compared with that in the liquid phase to probe into the effect of solvent environment on the catalytic activity of Cu catalyst. Further, the comparisons of the mechanism among Cu(0), Cu(I) and Cu(II) catalysts are carried out to illustrate the effect of Cu valence state. The results are expected to provide a guide for the rational design of efficient Cu-based catalysts by tuning the catalyst valence state and solvent environments in the oxidative carbonylation of methanol.

2. Computational details

2.1. Surface models

In the case of CuO unit cell, each atom has four nearest neighbors of another species; oxygen atom is surrounded by a distorted tetrahedron of Cu atoms while each Cu atom is surrounded by a square of oxygen atoms [48]. The structure, stability and adsorption properties of CuO (111) surface have been investigated using DFT calculations [48–52], suggesting that the (111) surface is the most stable under the realistic conditions, which is also confirmed by the X-ray diffraction [53–55].

As shown in Fig. 1, a six-layer $p(3 \times 2)$ CuO(111) surface is used to model Cu(II) catalyst, which corresponds to the coverage of 1/6 ML. The vacuum space of 10 Å is added perpendicular to the surface to avoid the interactions between the slabs. In all calculations, the top three layers and the adsorbed species are allow to relax, while the bottom three layers are fixed to maintain the bulk crystal structure. CuO(111) surface includes eight adsorption sites: Cu_{SUF}(I), Cu_{SUB}(II), O_{SUF}(III), O_{SUB}(IV), Cu_{SUB}–Cu_{SUB} bridge(V), O_{SUB}–O_{SUB} bridge(VI), O_{SUF}–O_{SUF} bridge(VII) and Cu_{SUF}–Cu_{SUF} bridge sites(VIII). Cu_{SUF}(I) and O_{SUF}(III) sites are the surface Cu and O atoms, respectively; Cu_{SUB}(II) and O_{SUB}(IV) sites are the subsurface Cu and O atoms, respectively [56].

2.2. Calculation methods

All DFT calculations are performed with Dmol^3 program in Materials Studio 8.0 [57,58]. The exchange-correlation functional was constructed by the GGA of Perdew and Wang (PW91) [59–61]. Spin-unrestricted is used. In the computation, the inner electrons of Cu atoms are kept frozen and replaced by a DFT Semi-core Pseudopots (DSPP) [62,63]; other atoms are treated with an all-electron basis set. The valence electrons functions are expanded into a set of numerical atomic orbital by a double-numerical basis with polarization functions (DNP) [62–64]. Brillouin-zone integrations have been performed using $3 \times 3 \times 1$ Monkhorst-Pack grid and a Methfessel–Paxton smearing of 0.005 Ha [50]. The convergence criteria of SCF was 1×10^{-5} Ha; the converge criterion of geometry optimization and judged by the energy, force, displacement were 2×10^{-5} Ha, 4×10^{-3} Ha/Å, 5×10^{-3} Å, respectively; the convergence tolerance of TS search was obtained using the medium quality of 1×10^{-2} Ha/Å.

The conductor-like screening model (COSMO) implemented into the Dmol^3 has been used to simulate the solvent effect [65–69]. In this model, the solute is put in the continuous medium where the dielectric constant is ε, the methanol and water solvent environments are replaced with the permittivity $\varepsilon = 32.63$ and 78.54. The transition states (TS) of elementary reactions are searched by complete linear synchronous transit and quadratic synchronous transit (LST/QST) method [70,71]. Meanwhile, a vibrational frequency analysis is calculated to validate the true nature of the saddle point by identifying only one imaginary frequency along the reaction coordinate, and TS confirmation is performed on every transition state to confirm that they lead to the desired reactants and products.

3. Results and discussion

3.1. Evaluation of the method and model

In order to verify the credibility of calculation method and model, the bulk lattice parameters of CuO is firstly calculated, a = 4.684 Å, b = 3.423 Å, c = 5.129 Å and β = 99.54°, which agree with the experimental values [72] of a = 4.653 Å, b = 3.410 Å, c = 5.108 Å and β = 99.50°. Then, the calculated C—O bond length of gas phase CO is 1.141 Å, which is close to the experimental value of 1.128 Å [73]. Above test results show that the method and model employed in this study are reliable to describe the mechanism and kinetics of DMC formation on CuO catalyst.

3.2. The adsorption of the species involved in DMC formation

The adsorption energy (E_{ads}) is used to measure the interaction strength between the adsorbate and the substrate, which is obtained by

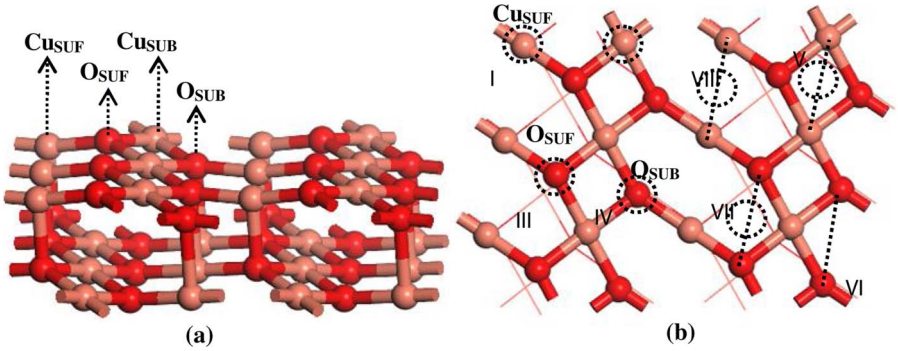

Fig. 1. The slab model of a $p(3 \times 2)$ CuO(111) surface. (a) Side view, (b) Top view. Orange and red balls stand for Cu and O atoms, respectively. (For interpretation of the references to colour in this figure legend, the reader is referred to the web version of this article.)

Table 1
Adsorption energies and key structural parameters for the most stable configurations of adsorbed species involving in DMC formation over CuO(111) surface in the gas phase.

Species	Site	Mulliken charge (e)	E_{ads} (kJ mol^{-1})	$d_{Cu\text{-}X}$ (Å)	
				This study	Ref. [25]
CO	Cu_{sub}: via C	0.393	70.5	1.916	–
CH_3O	Cu_{sub}- Cu_{sub}: via O	−0.136	189.9	2.012, 2.014	2.070, 2.029
O	Cu_{sub}-Cu_{sub}: via O	−0.476	272.1	1.868, 1.862	1.889, 1.893
OH	Cu_{sub}-Cu_{sub}: via O	−0.183	254.8	1.991, 1.999	1.991, 2.057
CH_3OH	Cu_{sub}: via O	0.233	94.4	2.113	2.252
CH_3OCO	Cu_{sub}: via C	0.298	204.5	1.928	–
DMC	Cu_{sub}-Cu_{sub}: via O	0.129	22.4	2.517, 2.523	–

the following equation:

$$E_{ads} = E_{sub} + E_{mol}\text{-}E_{mol/sub}$$

E
mol/sub
–
E
sub
E
mol
E
ads

The adsorption of all species involved in DMC formation under different solvent conditions are examined over the eight adsorption sites of CuO(111) surface. Only the most stable adsorption configurations are considered; the adsorption energies and key structural parameters are listed in Tables 1 and 2.

3.2.1. In the gas phase

As shown in Fig. 2, CH_3OH, CH_3O, O and OH species prefer to be adsorbed at the Cu_{SUB}, Cu_{SUB}-Cu_{SUB}, Cu_{SUB}-Cu_{SUB} and Cu_{SUB} sites, respectively, which agree with the previous results [49]. The corresponding adsorption energies are 94.4, 189.9, 272.1 and 254.8 kJ mol^{-1}, respectively.

CO prefers to be adsorbed at the Cu_{SUB} site, which has the adsorption energy of 70.5 kJ mol^{-1}, and the corresponding charge transfer from CO to the surface is 0.393 *e*; the length of C—Cu bond is 1.916 Å. CH_3OCO is located at the Cu_{SUB} site via carbonyl C atom with an adsorption energy of 204.5 kJ mol^{-1}; the corresponding charge transfer from CH_3OCO to the surface is 0.298 *e*, and the C-Cu_{SUB} bond length is 1.928 Å. In the case of DMC, the adsorption energies at different adsorption sites are close, that at the Cu_{SUB}-Cu_{SUB} bridge site has relatively large adsorption energy of 22.4 kJ mol^{-1}, and the charge transfer from DMC to the surface is 0.129 *e*.

3.2.2. In the liquid phase

As listed in Table 2, CO prefers to adsorbed at the Cu_{SUB} site in methanol and water with the adsorption energies of 70.1 and 70.4 kJ mol^{-1}, respectively; the charge transfer from CO to the surface is 0.384 and 0.393 *e*, respectively. For other species, the stable adsorption configurations in methanol and water solvents are similar with those in the gas phase, as shown in Fig. 2.

Above results clearly showed that the Cu_{SUB} and Cu_{SUB}-Cu_{SUB} are the most favorable adsorption site for all species involved in DMC formation over CuO(111) surface; solvent effects only slightly change the stable adsorption configurations of adsorbed species, and slightly weaken the adsorption ability of adsorbed species.

3.3. Reaction mechanism

Based on the previous studies [11,31], the proposed mechanism for DMC formation via the oxidative carbonylation of methanol is shown in Scheme 1, and every reaction is demonstrated by experiment [34,74]. An asterisk presents the active site, and (X)* stands for the species X interacting with the active site.

In this study, the mechanism of DMC formation under different environments is investigated, the related structural parameters, adsorption energies, reaction energies, and activation barriers are obtained to probe into the effects of Cu valence state and solvent environment on the mechanism and kinetics of DMC formation.

3.3.1. The mechanism of DMC formation in the gas phase

3.3.1.1. (A) CH_3O formation by CH_3OH dissociation in the presence of oxygen. Previous studies [31] have suggested that the presence of oxygen can promote the CH_3OH dehydrogenation to CH_3O over Cu_2O catalyst. Sun et al. [49] have calculated the Reactions 1 and 2 over the oxygen-precovered CuO(111) surface, suggesting that the presence of oxygen significantly promotes CH_3OH dehydrogenation to CH_3O. Our calculated results show that CH_3OH dissociation into CH_3O is spontaneous in the presence of precovered-oxygen over CuO(111) surface, it is strongly exothermic by 108.6 kJ mol^{-1}. Thus, it is reasonable to assume that the formation of $(CH_3O)^*(OH)^*$ can rapidly occur, namely, when the oxygen exists in the feed, the molecularly adsorbed CH_3OH is converted rapidly to CH_3O species.

3.3.1.2. (B) The formation of dimethoxide species. The intermediate

Table 2
Adsorption energies and key structural parameters for the most stable configurations of adsorbed species involving in DMC formation over CuO(111) surface in methanol and water solvents.

Species	Site	Mulliken charge (*e*)		E_{ads} (kJ mol^{-1})		$d_{Cu\text{-}X}$ (Å)	
		methanol	water	methanol	water	methanol	water
CO	Cu_{SUB}: via C	0.384	0.393	70.1	70.4	1.930	1.913
CH_3O	Cu_{SUB}-Cu_{SUB}: via O	−0.136	−0.136	177.1	177.5	2.012, 2.009	2.014, 2.010
O	Cu_{SUB}-Cu_{SUB}: via O	−0.476	−0.476	282.4	283.7	1.876, 1.862	1.876, 1.871
OH	Cu_{SUB}-Cu_{SUB}: via O	−0.187	−0.188	243.2	242.8	1.997, 2.003	1.999, 2.003
CH_3OH	Cu_{SUB}: via O	0.240	0.241	88.0	87.9	2.079	2.073
CH_3OCO	Cu_{SUB}: via O	0.297	0.438	195.6	195.3	1.932	1.938
DMC	Cu_{SUB}-Cu_{SUB}: via O	0.144	0.163	10.4	8.9	2.481, 2.482	2.443, 2.439

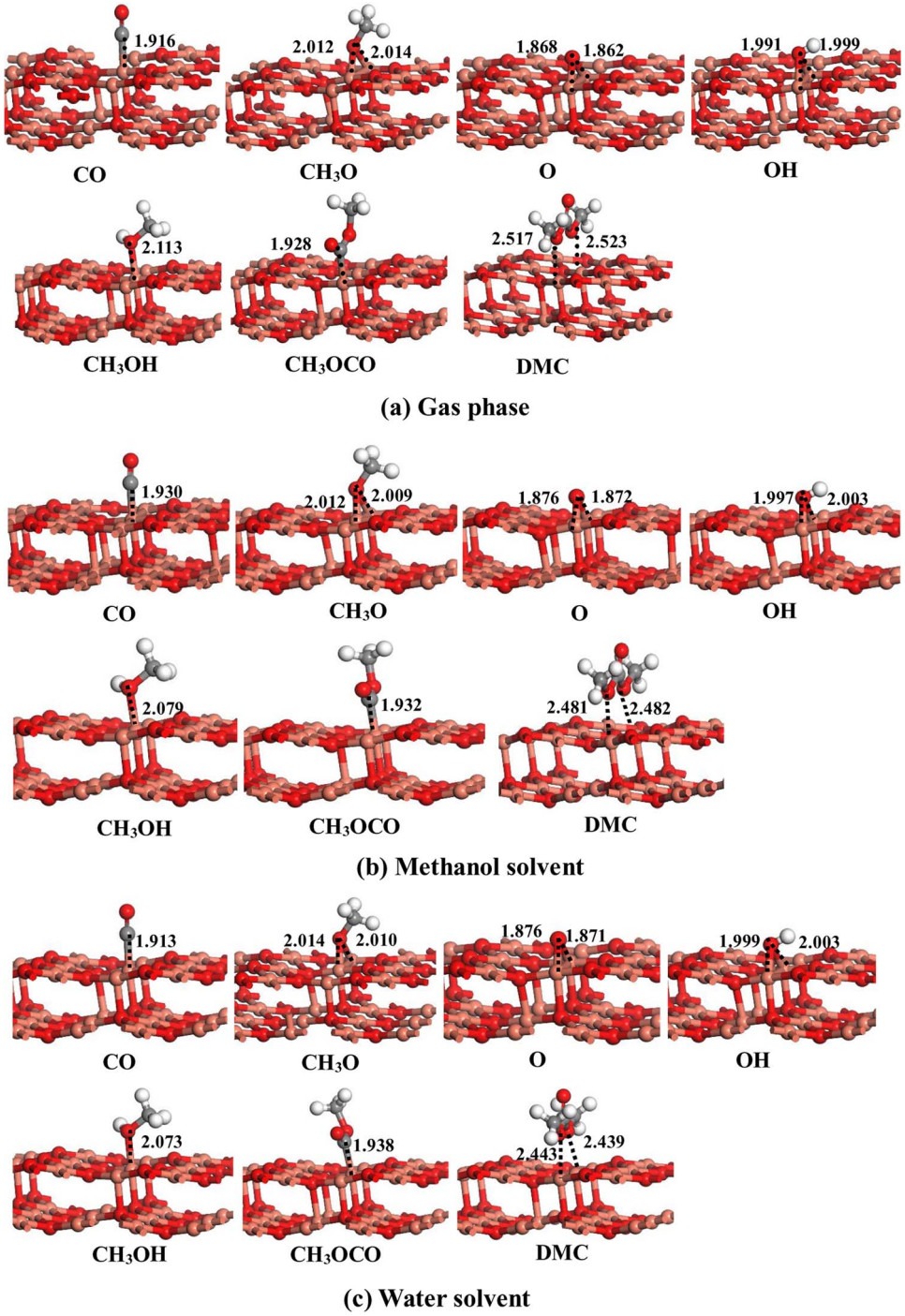

Fig. 2. The most stable adsorption configurations of the species involving in DMC formation over CuO(111) surface under different environments. White, grey black balls represent H and C atoms, respectively. Bond length is in Å.

	$CH_3OH+*\rightarrow(CH_3OH)*$	(1)
	$(CH_3OH)*+O*\rightarrow(CH_3O)*(OH)*$	(2)
Path 1	$(CH_3O)*(OH)*+(CH_3OH)*\rightarrow(CH_3O)_2*+(H_2O)*$	(3)
	$(CH_3O)_2*+(CO)\rightarrow(DMC)*$	(4)
Path 2	$(CH_3O)*+(CO)*\rightarrow(CH_3OCO)*$	(5)
	$(CH_3OCO)*+(CH_3O)*\rightarrow(DMC)*$	(6)
	$(DMC)*\rightarrow DMC+*$	(7)

Scheme 1. Two possible pathways involving in the mechanism of DMC formation by the oxidative carbonylation of methanol.

species dimethoxide $(CH_3O)_2*$ and H_2O can be formed in Reaction 3. The co-adsorbed configurations of $(CH_3O)*(OH)*$ and CH_3OH over CuO (111) surface are shown in Fig. 3(a), in which all species are adsorbed at the Cu_{SUB} site, the distance between the H atom of OH in CH_3OH and the O atom of OH* is 1.349 Å; the Mulliken charges of CH_3O*, OH*, and CH_3OH are −0.146, −0.269 and 0.242 *e*, respectively. Further, $(CH_3O)_2*$ is formed from the co-adsorbed $(CH_3O)*(OH)*$ and $(CH_3OH)*$ via the L-H (Langmuir–Hinshelwood) mechanism.

Starting from the co-adsorbed $(CH_3O)*(OH)*$ and $(CH_3OH)*$, $(CH_3O)_2*$ can be formed via the transition state TS1 (Fig. 3(b)). In TS1, the distance between the H atom of OH in CH_3OH and the O atom of OH decreases from 1.349 Å to 1.053 Å; the charges of CH_3O*, the formed

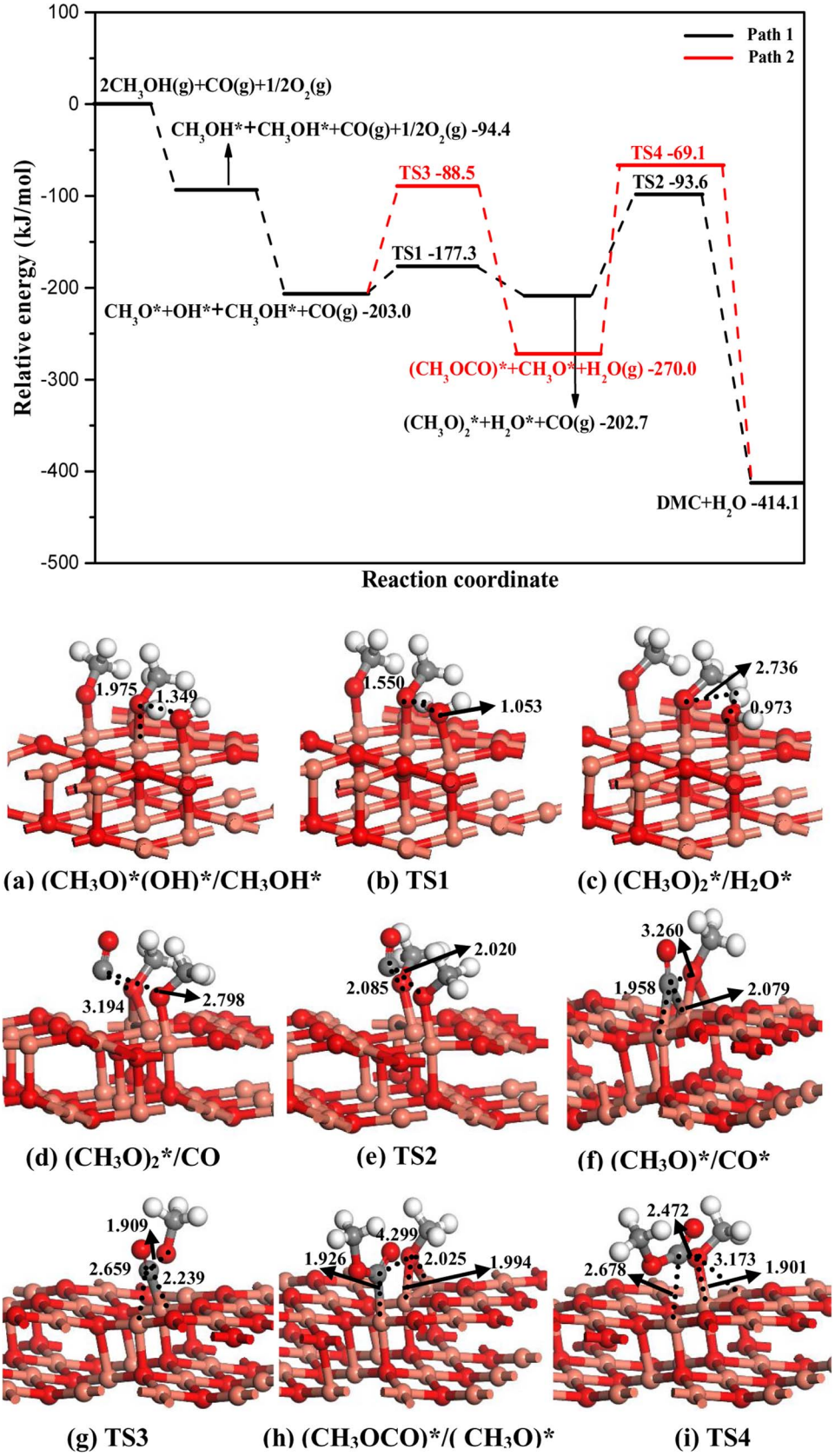

Fig. 3. The energy profiles for two pathways of DMC formation in the gas phase with the corresponding structures of co-adsorbed species and transition states over CuO(111) surface.

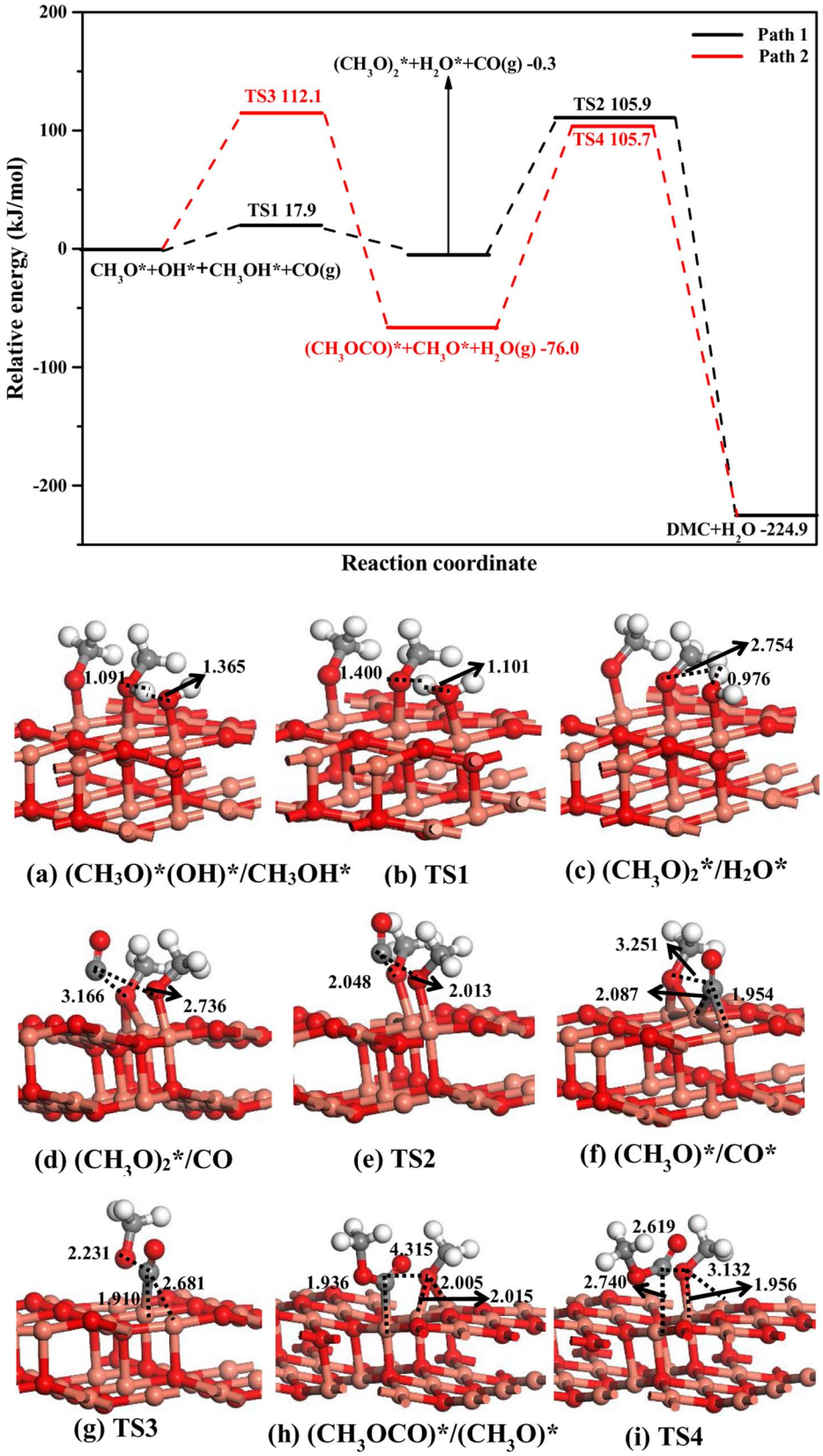

Fig. 4. The energy profiles for two pathways of DMC formation in methanol solvent with the corresponding structures of co-adsorbed species and transition states over CuO(111) surface.

H_2O and CH_3O^* are −0.195, 0.245 and −0.251 *e*, respectively. In $(CH_3O)_2^*/H_2O$ configuration (Fig. 3(c)), the bond length of new formed O—H is 0.973 Å, and the distance between the O atom of CH_3O^* and the H atom of H_2O is 2.736 Å; two CH_3O species and H_2O are adsorbed at the Cu_{SUB} site with the Mulliken charges of −0.250, −0.167 and 0.210 *e*, respectively. This reaction is slightly endothermic by 0.3 kJ mol^{-1} with an activation barrier of 25.7 kJ mol^{-1}.

3.3.1.3. (C) CO insertion into dimethoxide species to DMC. DMC can be formed by CO insertion into $(CH_3O)_2$* via the transition state TS2 in Reaction 4. In the co-adsorbed CO and $(CH_3O)_2$*, two CH_3O species prefers to occupy the Cu_{SUB}-Cu_{SUB} and Cu_{SUB} sites (Fig. 3(d)) since CH_3O adsorption is much stronger than CO (189.9 *vs.* 70.5 kJ mol^{-1}), which keeps CO away from CuO surface. The bond length of CO (1.141 Å) is same with that in gas phase (1.141 Å), the distance between the C atom of CO and the O atom of two CH_3O are 3.194 and 2.798 Å, respectively. The Mulliken charges show that two adsorbed CH_3O* are −0.150 and −0.161 *e*, but the charges of CO is only 0.084 *e*. These results proved that DMC is formed by gas phase CO insertion into the adsorbed $(CH_3O)_2$* over CuO(111) surface via the E-R (Eley-Rideal) mechanism.

In TS2 (Fig. 3(e)), one CH_3O* remove from the Cu_{SUB}-Cu_{SUB} to the Cu_{SUB} site, the other is still adsorbed at the Cu_{SUB} site. Moreover, the C—O bond length of CO is elongated from 1.141 Å to 1.173 Å, and the distance between C atom of CO and O atom of two CH_3O* decrease from 3.194 and 2.798 Å to 2.085 and 2.020 Å, respectively. Moreover, the Mulliken charges of CO and two CH_3O* molecules are 0.036, −0.162, and −0.146 *e*, respectively. This reaction is exothermic by 211.4 kJ mol^{-1}, and it has an activation barrier of 109.1 kJ mol^{-1}. Thus, CO insertion into dimethoxide species to DMC (Reaction 4) is the rate-limiting step of Path 1.

3.3.1.4. (D) CO insertion into methoxide species to CH_3OCO. The intermediate (CH_3OCO)* can be formed via TS3 with CO insertion into CH_3O in Reaction 5, the co-adsorbed configurations of CO and CH_3O in Fig. 3(f) indicate that both CO and CH_3O are adsorbed at the Cu_{SUB}-Cu_{SUB} sites. The distance between the O atom of CH_3O and the C atom of CO is 3.260 Å, the H_3CO-Cu_{SUB} distances are 1.939 and 2.097 Å, and the OC—Cu_{SUB} bond lengths are 1.958 and 2.079 Å. The Mulliken charges of CO and CH_3O are 0.315 and −0.142 *e*. these results demonstrate that (CH_3OCO)* can be formed with (CO)* insertion into (CH_3O)* via the L-H mechanism.

In TS3 (Fig. 3(g)), CO migrates to the Cu_{SUB} site from the Cu_{SUB}-Cu_{SUB} site, the distance between the C atom of CO and the O atom of CH_3O is 1.909 Å, and the Mulliken charge of CO is 0.309 *e*. Meanwhile, CH_3O leave away from the surface, and the H_3CO—Cu_{SUB} bond length greatly increased to 2.519 and 2.419 Å; the charge transfer from the surface to CH_3O in TS3 is 0.221 *e*. This reaction is exothermic by 67.0 kJ mol^{-1} with an activation barrier of 114.5 kJ mol^{-1}.

3.3.1.5. (E) Methoxide reacting with CH_3OCO to DMC. DMC can be formed by Path 2 via TS4 in Reaction 6, in the co-adsorbed configurations of (CH_3OCO)*/(OCH_3)* (Fig. 3(h)), (CH_3OCO)* occupy the Cu_{SUB} site with the C-Cu_{SUB} distance of 1.926 Å, and the Mulliken charge of CH_3OCO is 0.288 *e*. Meanwhile, (CH_3O)* is adsorbed at the Cu_{SUB}-Cu_{SUB} site with the O-Cu_{SUB} distance of 2.025 and 1.994 Å, respectively. The Mulliken charge of CH_3O is −0.140 *e*. The distance between the C atom of (CH_3OCO)* and the O atom of (OCH_3)* is 4.299 Å. Thus, DMC is formed by the adsorbed (CH_3OCO)* and (OCH_3)* species via the L-H mechanism.

In TS4 (Fig. 3(i)), CH_3OCO tend to leave the surface with the C-Cu_{SUB} distance of 2.678 Å, CH_3O species is immigrated to the Cu_{SUB} site with the O-Cu_{SUB} distance of 1.901 Å. As the reaction proceeds, the distance between the C atom of (CH_3OCO)* and the O atom of (OCH_3)* decrease to 2.472 Å. Moreover, the Mulliken charge of CH_3OCO and OCH_3 species are 1.685 and −0.125 *e*, respectively. This reaction is largely exothermic by 144.1 kJ mol^{-1} with an activation barrier of 200.9 kJ mol^{-1}. Above results show that Reaction 6 is the rate-limiting step for Path 2.

3.3.2. The mechanism of DMC formation in solvents

3.3.2.1. (A) The formation of dimethoxide species. Similar to that in gas phase, the intermediate (CH_3O)*(OH)* produced in Reaction 2 reacts further with (CH_3OH)* to form the dimethoxide species $(CH_3O)_2$* and H_2O*. The structures in methanol and water solvents are shown in Figs. 4 and 5. All species are adsorbed at the Cu_{SUB} site, the distances between the H atom of OH in CH_3OH and the O atom of OH* are 1.365 Å in methanol and 1.367 Å in water; the Mulliken charges of CH_3O*, OH* and CH_3OH* are −0.150, −0.270 and 0.230 *e* in methanol, and −0.150, −0.267 and 0.217 *e* in water. The results show that the dimethoxide species are formed via the L-H mechanism in two solvents.

In TS1 (Figs. 4(b) and 5(b)), the distance between the H atom of OH in CH_3OH and O atom of OH decreases to 1.101 Å in methanol and 1.052 Å in water; the charges of CH_3O*, the formed H_2O and CH_3O* are −0.170, 0.223 and −0.262 *e* in methanol, and −0.167, 0.241 and −0.286 *e* in water. In $(CH_3O)_2$*/H_2O configuration (Figs. 4(c) and 5(c)), CH_3O*, CH_3O* and H_2O are adsorbed at the Cu_{SUB} sites; the distances between the H atom of OH in CH_3OH and the O atom of OH are decreased in both methanol (0.976 Å) and water (0.976 Å); the corresponding Mulliken charges are −0.254, −0.166 and 0.213 *e* in methanol, and −0.246, −0.171 and 0.208 *e* in water. This reaction is slightly exothermic by 0.3 kJ mol^{-1} with an activation barrier of 17.9 kJ mol^{-1} in methanol; in water, it is exothermic by 4.4 kJ mol^{-1} with an activation barrier of 15.5 kJ mol^{-1}. Compared to that (25.7 kJ mol^{-1}) in the gas phase, solvent environments promote the formation of dimethoxide intermediates.

3.3.2.2. (B) CO insertion into dimethoxide species to DMC. CO insertion into $(CH_3O)_2$* can formed DMC via TS2 in Reaction 4, in $(CH_3O)_2$*/CO, two CH_3O* are adsorbed at the Cu_{SUB}-Cu_{SUB} and Cu_{SUB} sites (Figs. 4(d) and 5(d)). The bond length of CO (1.141 Å) in solvents is same with that in gas phase; the distance between the C atom of CO and the O atom of two CH_3O are 3.166 and 2.736 Å in methanol, those are 3.207 and 2.744 Å in water. The Mulliken charges of two CH_3O* and CO are −0.154, −0.158, and 0.081 *e* in methanol, those are −0.150, −0.166 and 0.087 *e* in water. These results show that DMC formation goes through the E-R mechanism in two solvents. In TS2 (Figs. 4(e) and 5(e)), one of CH_3O* transfers from the Cu_{SUB}-Cu_{SUB} to Cu_{SUB}, the other is still adsorbed at the Cu_{SUB} site. The distance between the C atom of CO and O atom of two CH_3O* decrease to 2.048 and 2.013 Å in methanol, those are 2.070 and 1.959 Å in water. The Mulliken charges of (CO)* and two CH_3O* are 0.052, −0.161, and −0.146 *e* in methanol, those are 0.061, −0.151, and −0.154 *e* in water. This reaction is exothermic by 224.6 kJ mol^{-1} with an activation barrier of 106.2 kJ mol^{-1} in methanol; however, it is exothermic by 217.8 kJ mol^{-1} with an activation barrier of 184.7 kJ mol^{-1} in water. Thus, the reaction 4 is still the rate-limiting step of Path 1.

3.3.2.3. (C) CO insertion into methoxide species to CH_3OCO. In the co-adsorbed configurations of (CH_3O)* and (CO)* in Figs. 4(f) and 5(f), both CO and CH_3O species occupy the Cu_{SUB}-Cu_{SUB} site, the distance between the O atom of CH_3O and the C atom of CO is 3.251 Å in methanol and 3.264 Å in water; The bond lengths of OC-Cu_{SUB} are 1.954 and 2.087 Å in methanol, 1.954 and 2.080 Å in water. The Mulliken charges of CO and CH_3O are 0.311 and −0.141 *e* in methanol, 0.311 and −0.147 *e* in water. Therefore, (CH_3OCO)* should be formed from (CH_3O)* and (CO)* in two solvents via the L-H mechanism.

The co-adsorbed (CH_3O)* and (CO)* can form (CH_3OCO)* via the transition state TS3 (Figs. 4(g) and 5(g)), this reaction is exothermic by 76.0 kJ mol^{-1} with an activation barrier of 112.1 kJ mol^{-1} in methanol, and it is exothermic by 66.6 kJ mol^{-1} with an activation barrier of 82.0 kJ mol^{-1} in water. In TS3, CH_3O species leaves from the CuO (111) surface with the charge transferred from surface to CH_3O is 0.212 *e* in methanol and 0.229 *e* in water. Meanwhile, CH_3O species approaches the adsorbed (CO)*, the distance between the O atom of CH_3O and the C atom of CO decrease to 2.231 Å in methanol and 2.185 Å in water; the Mulliken charge of CO is 0.309 *e* in methanol and 0.299 *e*.

3.3.2.4. (D) Methoxide reacting with CH_3OCO to DMC. DMC can be

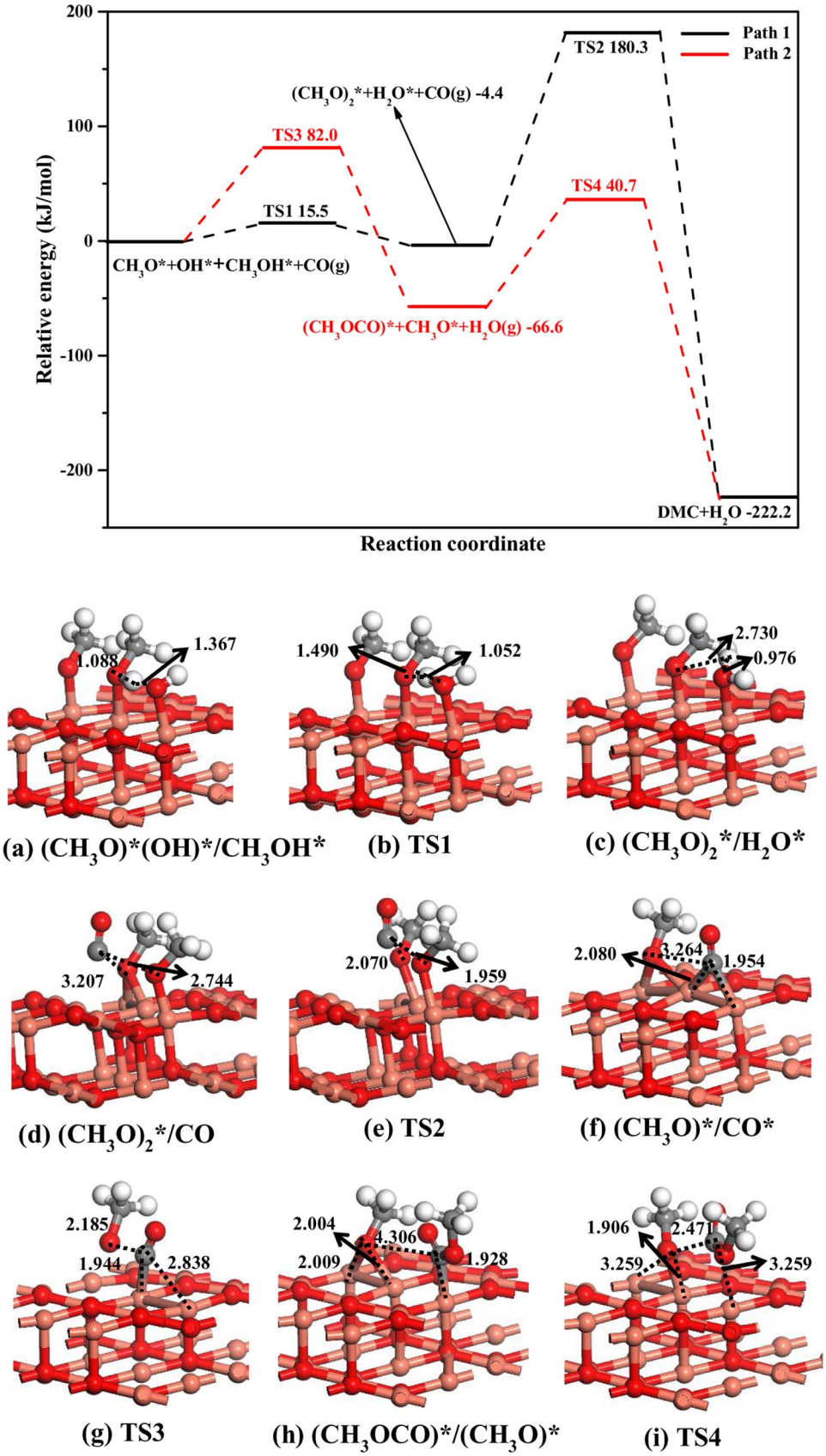

Fig. 5. The energy profiles for two pathways of DMC formation in water solvent with the corresponding structures of co-adsorbed species and transition states over CuO(111) surface.

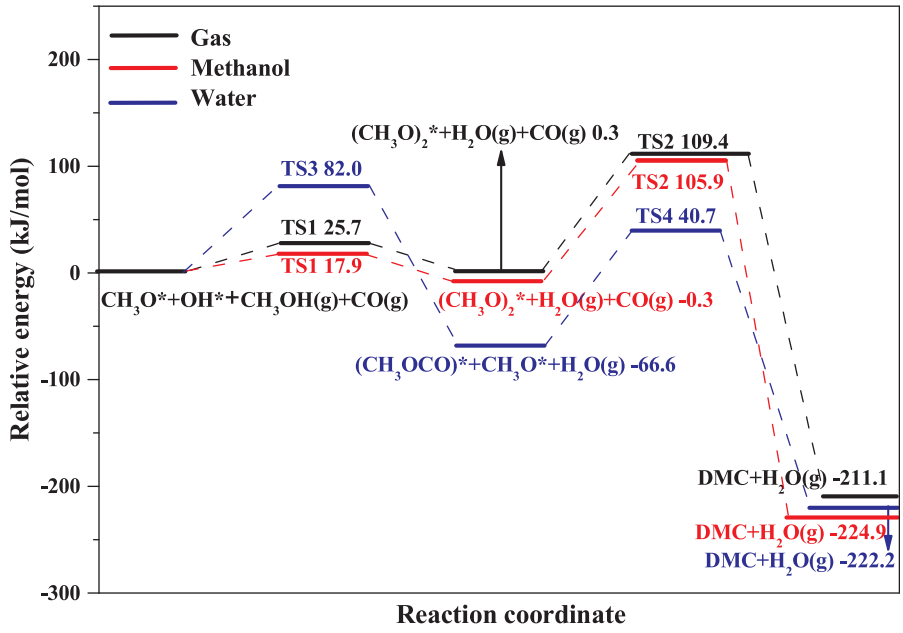

Fig. 6. The energy profiles for the most favorable pathways of DMC formation over CuO catalyst in different solvents.

formed by (CH_3OCO)* interacting with another (OCH_3)* species via TS4. In the co-adsorbed configurations of (CH_3OCO)*/(OCH_3)* in Figs. 4(h) and 5(h), the distance between the C atom of (CH_3OCO)* and the O atom of (OCH_3)* is 4.315 Å in methanol and 4.306 Å in water. (CH_3OCO)* occupy the Cu_{SUB} site with a C-Cu_{SUB} distance of 1.936 Å in methanol and 1.928 Å in water. The Mulliken charge of CH_3OCO is 0.288 *e* in methanol and 0.292 *e* in water. Meanwhile, CH_3O is adsorbed at the Cu_{SUB}-Cu_{SUB} site with the O-Cu_{SUB} distance of 2.015 and 2.005 Å in methanol, 2.009 and 2.004 Å in water; the Mulliken charge of CH_3O is −0.142 *e* in methanol and −0.137 *e* in water. Thus, DMC is formed by adsorbed (CH_3OCO)* and (OCH_3)* species via the L-H mechanism in two solvents.

In TS4 (Figs. 4(i) and 5(i)), CH_3OCO tends to leave the surface with the C-Cu_{SUB} distance of 2.740 Å in methanol and 3.259 Å in water; CH_3O species transfers to the Cu_{SUB} site with the O-Cu_{SUB} distance of 1.956 Å in methanol and 1.906 Å in water. The distance between the α-C atom of (CH_3OCO)* and the O atom of (CH_3O)* decreases to 2.619 Å in methanol and 2.471 Å in water. Moreover, the Mulliken charge of CH_3OCO and OCH_3 species are 0.235 and −0.160 *e* in methanol, 0.206 and −0.139 *e* in water. As the reaction proceeds, CH_3OCO approaches CH_3O to form DMC. This reaction is exothermic by 148.9 kJ mol^{-1}, which has an activation barrier of 181.7 kJ mol^{-1} in methanol. However, the activation barrier is lower in water (107.3 kJ mol^{-1}), and it is exothermic by 155.6 kJ mol^{-1}. Thus, Reaction 6 is the rate-limiting step of Path 2 for DMC formation.

3.4. General discussion

3.4.1. The mechanism of DMC formation over CuO(111) surface in the gas phase

As shown in Fig. 3, starting from CH_3O* + OH* + CH_3OH* + CO (g) species, the highest barrier of Path 1 including Reactions 3 and 4 (−93.6 kJ mol^{-1}) is lower than that of Path 2 consisted of Reactions 5 and 6 (−69.1 kJ mol^{-1}); moreover, the rate-limiting step of Path 1, CO insertion into $(CH_3O)_2$*, has lower activation barrier than that of Path 2 with CH_3O interacting with CH_3OCO to DMC (109.1 *vs.* 200.9 kJ mol^{-1}). These results suggest that Path 1 via CO insertion into $(CH_3O)_2$ dominantly contribute to DMC formation instead of Path 2 via CO insertion into CH_3O to CH_3OCO, followed by interacting with CH_3O to DMC.

3.4.2. The effects of solvent environment on the mechanism of DMC formation

Starting from CH_3O* + OH* + CH_3OH* + CO(g) species, in methanol solvent, as shown in Fig. 4, the highest barrier of Path 1 (105.9 kJ mol^{-1}) is slightly lower than that of Path 2 (112.1 kJ mol^{-1}). However, CO insertion into $(CH_3O)_2$*, the rate-limiting step of Path 1, has much lower activation barrier than that of Path 2 with CH_3O interacting with CH_3OCO to DMC (106.2 *vs.* 181.7 kJ mol^{-1}). Thus, in methanol solvent, Path 1 via CO insertion into $(CH_3O)_2$ still contribute to DMC formation instead of Path 2 via CO insertion into CH_3O to CH_3OCO, followed by interacting with CH_3O to DMC.

Similarly, as shown in Fig. 5, in water solvent, the highest barrier of Path 1 (180.3 kJ mol^{-1}) is much higher than that of Path 2 (82.0 kJ mol^{-1}); moreover, CO insertion into $(CH_3O)_2$*, the rate-limiting step of Path 1, has much higher activation barrier than that of Path 2 with CH_3O interacting with CH_3OCO to DMC (184.7 *vs.* 107.3 kJ mol^{-1}). Thus, in water solvent, Path 2, CO insertion into CH_3O to CH_3OCO, followed by interacting with CH_3O to DMC, is dominantly responsible for DMC formation instead of Path 1 via CO insertion into $(CH_3O)_2$, which is different from those in the gas phase and methanol solvent.

It is noted that COSMO model could effectively treat the long-range solvent effect, however, the short-range solvent effect between methanol as the reactant in DMC formation and the water or methanol solvents, such as the hydrogen-bonding interaction may affect the DMC formation [65,66]. To further explore the short-range effect, explicit solvent molecules are considered for the reaction 5 in water solvent and the reaction 4 in methanol solvent; the corresponding structures of these two reactions are shown in Figs. S1 and S2 . The results show that when DMC is formed in water solvent, the activation barriers of the reaction 5 is higher than that using COSMO long-range solvent effect (99.7 *vs.* 82.0 kJ mol^{-1}), and it is exothermic by 78.2 and 66.6 kJ mol^{-1}, respectively. Similarly, in methanol solvent, the activation barriers of the reaction 5 is higher than that using COSMO long-range solvent effect (120.2 *vs.* 106.2 kJ mol^{-1}), and it is exothermic by 214.6 and 224.6 kJ mol^{-1}, respectively. The above results indicate that compared to that using COSMO model, the results obtained by the short-range solvent effect has some effect on the activation barriers and reaction energies of above two reactions in solvent environment. Thus, the short-range solvent effect should be also considered in our next work; only the long-range solvent effect using COSMO model is

examined in this study.

Above results show that the solvent environment has a significant effect on the mechanism of DMC formation; moreover, as shown in Fig. 6, the solvent environment also has a significant effect on the kinetics of DMC formation, especially when the reaction of DMC formation is carried out in water solvent, DMC formation is the most favorable, which has only the highest barrier of 82.0 kJ mol^{-1}. Our previous studies about the effects of solvent on reaction kinetics of DMC formation over $Cu_2O(111)$ also indicated that the solvent effect can improve the performance of DMC formation in a liquid-phase slurry [31]. Thus, it is concluded that tuning the reaction environments can improve the catalytic performance of the catalyst.

3.4.3. The effects of Cu valence state on the mechanism of DMC formation

For Cu(II) catalyst, above results suggest that Path 1 is the most favorable pathway of DMC formation via CO insertion into $(CH_3O)_2$* species, CO insertion into $(CH_3O)_2$* is the rate-limiting step. Previous DFT studies by Meng et al. [35,75] have investigated the oxidative carbonylation of methanol over $CuCl_2$–$PdCl_2$ bimetallic catalyst (Wacker-type catalyst), which also suggest that DMC is dominantly formed via CO insertion into $(CH_3O)_2$* species. Further, previous experimental studies [38–40,76–78] have demonstrated that Cu(II) should be also the active species in DMC formation, such as the studies by Wang et al. [76] indicated that compared to the conventional Cu^I/Y catalyst, the catalyst prepared by $CuCl_2$ and HY zeolite possess higher activity for the oxidative carbonylation of methanol, in which the active species CuCl and $CuCl_2$ were co-exist. Sato et al. [40,77] and Du et al. [78] also suggested that Cu(II) coordination compounds exhibited the high activity for the oxidative carbonylation of methanol to DMC.

For Cu(I) catalyst, our previous DFT studies [31] show that Path 2 is the most favorable pathway of DMC formation via CO insertion into CH_3O to CH_3OCO, followed by interacting with CH_3O to DMC, and CO insertion into CH_3O to CH_3OCO is the rate-limiting step. King et al. [32] studied the reaction mechanism by in-situ FTIR, which showed that CO insertion into copper methoxide is the most favorable step over solid-state ion-exchanged CuY catalysts. Shen et al. [36] found that CO insertion is the rate-limiting step for both pathways of DMC formation over Cu(I)/β catalyst, and both paths competitively occur in the reaction course.

For Cu(0) catalyst, Ren et al. [79] have carried out a detailed DFT investigation for DMC formation on Cu^0/AC catalyst, indicating that CO insertion into dimethoxide and methoxide are the rate-limiting steps for two pathways of DMC formation, and the preferred pathway of DMC formation is CO insertion into methoxide to CH_3OCO, followed by its interaction with another CH_3O to DMC species.

Thus, when the mechanism of DMC formation via oxidative carbonylation of methanol are compared among different valence states of Cu catalyst, Cu valence state also has a significant effect on the mechanism of DMC formation; however, CO insertion is the rate-limiting step over different valence state of Cu catalysts.

4. Conclusions

In this study, in order to probe into the effects of Cu valence state and solvent environments on the mechanism and kinetics of DMC formation over Cu catalyst, the mechanism and kinetics of DMC formation on Cu(II) catalyst in the gas phase, methanol and water solvents have been fully investigated using density functional theory calculations; then, the obtained results are compared with those over Cu(0) and Cu(I) catalysts. The results show that compared to the kinetics of DMC formation in the gas phase, the solvent in the liquid phase can improve the catalytic activity of Cu(II) and Cu(I) catalysts towards DMC formation in a liquid-phase slurry, especially in water. Moreover, the comparisons for the most favorable pathway of DMC formation among different valence state of Cu catalysts indicate that Cu valence state has a significant effect on DMC formation mechanism. The results provide a clue to finely tune the catalytic activity of DMC formation over Cu-based catalyst using the valence state and solvent environments under the realistic conditions.

Acknowledgments

This work is financially supported by the National Natural Science Foundation of China (No. 21476155, 21776193, 21576178), the Key Projects of National Natural Science Foundation of China (21736007), the China Scholarship Council (201606935026), the Program for the Top Young Academic Leaders of Higher Learning Institutions of Shanxi, the Top Young Innovative Talents of Shanxi.

Appendix A. Supplementary data

Supplementary data associated with this article can be found, in the online version, at http://dx.doi.org/10.1016/j.mcat.2018.02.005.

References

[1] P. Tundo, M. Selva, Acc. Chem. Res. 35 (2002) 706–716.
[2] F. Aricò, P. Tundo, Russ. Chem. Rev. 79 (2010) 479–489.
[3] A.H. Tamboli, A.A. Chaugule, H. Kim, Chem. Eng. J. 323 (2017) 530–544.
[4] D. Delledonne, F. Rivetti, U. Romano, Appl. Catal. A: Gen. 221 (2001) 241–251.
[5] M. Wang, N. Zhao, Y. Sun, Ind. Eng. Chem. Res. 44 (2005) 7596–7599.
[6] H. Lin, B. Yang, J. Sun, X. Wang, D. Wang, Chem. Eng. J. 103 (2004) 21–27.
[7] F.P. Documents, United States Patent 191, 1987.
[8] J. Bian, X.W. Wei, Y.R. Jin, L. Wang, Chem. Eng. J. 165 (2010) 686–692.
[9] X.L. Wu, M. Xiao, Y.Z. Meng, Y.X. Lu, J. Mol. Catal. A: Chem. 238 (2005) 158–162.
[10] K. Almusaiteer, Catal. Commun. 10 (2009) 1127–1131.
[11] X.B. Zheng, A.T. Bell, J. Phys. Chem. C 112 (2008) 5043–5047.
[12] S.A. Anderson, T.W. Root, J. Catal. 217 (2003) 396–405.
[13] J. Ren, S.S. Liu, Z. Li, X.L. Lu, K.C. Xie, Appl. Catal. A: Gen. 366 (2009) 93–101.
[14] G. Merza, B. László, A. Oszkó, G. Pótári, K. Baán, A. Erdőhelyi, J. Mol. Catal. A: Chem. 393 (2014) 117–124.
[15] M.A. Pacheco, C.L. Marshal, Energ. Fuel 11 (1997) 2–29.
[16] Y.J. Wang, R.X. Jiang, X.Q. Zhao, S.F. Wang, J. Nat. Gas Chem. 9 (2000) 205–212.
[17] Y.H. Zhang, D.N. Briggs, E. Smit, A.T. Bell, J. Catal. 251 (2007) 443–452.
[18] K.T. Jung, A.T. Bell, Top. Catal. 20 (2002) 1–4.
[19] S.T. King, M.E. Jones, M.M. Olken, Production of dimethyl carbonate using copper zeolite catalysts, U.S. Patent, 1803, 1995.
[20] W.S. Dong, X.S. Zhou, C.S. Xin, C.L. Liu, Z.T. Liu, Appl. Catal. A: Gen. 334 (2008) 100–105.
[21] Y.H. Zhang, I.J. Drake, D.N. Briggs, A.T. Bell, J. Catal. 244 (2006) 219–226.
[22] S.T. King, J. Catal. 161 (1996) 530–538.
[23] V. Raab, M. Merz, J. Sundermeyer, J. Mol. Catal. A: Chem. 175 (2001) 51–63.
[24] X.S. Ding, X.M. Dong, D.T. Kuang, S.F. Wang, X.Q. Zhao, Y.J. Wang, Chem. Eng. J. 240 (2014) 221–227.
[25] M. Richter, M. Fait, R. Eckelt, M. Schneider, J. Radnik, D. Heidemann, R. Fricke, J. Catal. 245 (2007) 11–24.
[26] J. Engeldinger, C. Domke, M. Richter, U. Bentrup, Appl. Catal. A: Gen. 382 (2010) 303–311.
[27] M. Richter, M.J.G. Fait, R. Eckelt, E. Schreier, M. Schneider, M.M. Pohl, R. Fricke, Appl. Catal. B: Environ. 73 (2007) 269–281.
[28] S.A. Anderson, T.W. Root, J. Mol. Catal. A: Chem. 220 (2004) 247–255.
[29] I.J. Drake, Y.H. Zhang, D. Briggs, B. Lim, T. Chau, A.T. Bell, J. Phys. Chem. B 110 (2006) 11654–11664.
[30] Y.H. Zhang, I.J. Drake, A.T. Bell, Chem. Mater. 18 (2006) 2347–2356.
[31] R.G. Zhang, L.Z. Song, B.J. Wang, Z. Li, J. Comput. Chem. 33 (2012) 1101–1110.
[32] S.T. King, Catal. Today 33 (1997) 173–182.
[33] J. Engeldinger, M. Richter, U. Bentrup 14 (2012) 2183–2191.
[34] Y.H. Zhang, A.T. Bell, J. Catal. 255 (2008) 153–161.
[35] Q. Meng, S. Wang, Y. Shen, B. Yan, Y. Wu, X. Ma, Appl. Surf. Sci. 292 (2014) 117–127.
[36] Y. Shen, Q. Meng, S. Huang, S. Wang, J. Gong, X. Ma, RSC Adv. 2 (2012) 7109–7119.
[37] H. Zhang, S. Wang, X. Zhao, Y. Wang, J. Hebei Univ. Technol. 33 (2004) 36–40.
[38] Y.J. Wang, X.Q. Zhao, B.G. Yuan, B.C. Zhang, J.S. Cong, Appl. Catal. A: Gen. 171 (1998) 255–260.
[39] K. Tomishige, T. Sakaihori, S. Sakai, K. Fujimoto, Appl. Catal. A: Gen. 181 (1999) 95–102.
[40] Y. Sato, Y. Souma, Catal. Surv. JPN 4 (2000) 65–74.
[41] E.F. Lima, J.W. Carneiro, C. Fenollar-Ferrer, S. Miertus, S. Zinoviev, N.C. Tapanes, D.A. Aranda, Fuel 89 (2010) 685–690.
[42] Z.J. Zuo, W. Huang, P.D. Han, Z.H. Li, Appl. Surf. Sci. 256 (2010) 2357–2362.
[43] N.E. Hall, B.J. Smith, Solvation effects on zwitterion formation, J. Phys. Chem. A 102 (1998) 3985–3990.
[44] D. Jacquemin, J. Preat, E.A. Perpète, Chem. Phys. Lett. 410 (2005) 254–259.
[45] N. Sanna, G. Chillemi, A. Grandi, S. Castelli, A. Desideri, V. Barone, J. Am. Chem. Soc. 127 (2005) 15429–15436.

[46] J. Tomasi, B. Mennucci, R. Cammi, Chem. Rev. 105 (2005) 2999–3094.
[47] D. Jacquemin, E.A. Perpete, G. Scalmani, M.J. Frisch, I. Ciofini, C. Adamo, Chem. Phys. Lett. 421 (2006) 272–276.
[48] S.J. Sun, D.S. Zhang, C.Y. Li, Y.J. Wang, J. Chem. Eng. 258 (2014) 128–135.
[49] S.J. Sun, Y.J. Wang, Q.S. Yang, Appl. Surf. Sci. 313 (2014) 777–783.
[50] S.J. Sun, C.Y. Li, D.S. Zhang, Y.J. Wang, Appl. Surf. Sci. 333 (2015) 229–234.
[51] S.J. Sun, D.S. Zhang, C.Y. Li, Y.J. Wang, RSC Adv. 5 (2015) 21806–21811.
[52] J. Zhang, R.G. Zhang, B.J. Wang, L.X. Ling, Appl. Surf. Sci. 364 (2016) 758–768.
[53] T. Kyotani, H. Kawashima, A. Tomita, Environ. Sci. Technol. 23 (1989) 218–223.
[54] H.T. Hsueh, S.J. Chang, F.Y. Hung, W.Y. Weng, C.L. Hsu, T.J. Hsueh, S.S. Lin, B.T. Daic, J. Electrochem. Soc. 158 (2011) J106–J109.
[55] V. Oison, H. Ouali, C. Lambert-Mauriat, M. Freyss, Surf. Sci. 622 (2014) 44–50.
[56] A. Filippetti, V. Fiorentini, Phys. Rev. Lett. 95 (2005) 086405.
[57] B. Delley, J. Chem. Phys. 92 (1990) 508–517.
[58] B. Delley, J. Chem. Phys. 113 (2000) 7756–7764.
[59] J.P. Perdew, K. Burke, M. Ernzerhof, Phys. Rev. Lett. 77 (1996) 3865–3868.
[60] P. Hu, D.A. King, S. Crampin, M.H. Lee, M.C. Payne, Chem. Phys. Lett. 230 (1994) 501–506.
[61] J.P. Perdew, Y. Wang, Phys. Rev. B: Condens. Matter 45 (1992) 13244–13249.
[62] P. Hohenberg, W. Kohn, Phys. Rev. 136 (1964) B864–B871.
[63] Y. Inada, H. Orita, J. Comput. Chem. 29 (2008) 225–232.
[64] T.A. Halgren, W.N. Lipscomb, Chem. Phys. Lett. 49 (1977) 225–232.
[65] A. Klamt, G. Schüürmann, J. Chem. Soc. Perkin Trans. 2 (1993) 799–805.
[66] A. Klamt, V. Jonas, T. Bürger, J.C. Lohrenz, J. Phys. Chem. A 102 (1998) 5074–5085.
[67] T. Todorova, B. Delley, Mol. Simulat. 34 (2008) 1013–1017.
[68] A.V. Gavrilenko, T.D. Matos, C.E. Bonner, S.S. Sun, C. Zhang, V. Gavrilenko, J. Phys. Chem. C 112 (2008) 7908–7912.
[69] R.G. Zhang, X.B. Hao, T. Duan, B.J. Wang, Fuel Process. Technol. 156 (2017) 253–264.
[70] J.P. Perdew, Phys. Rev. B: Condens Matter 33 (1986) 8822–8824.
[71] J. Song, X. Niu, L. Ling, B. Wang, Fuel Process. Technol. 115 (2013) 26–33.
[72] S. Asbrink, L.J. Norrby, Acta Crystallogr. B 26 (1970) 8–15.
[73] J.X. Shao, X.L. Cheng, X.D. Yang, F.P. Zhang, S.H. Ge, J. At. Mol. Phys. 23 (2006) 80–84.
[74] Z.J. Zuo, L. Wang, P.D. Han, W. Huang, Int. J. Hydrogen Energ. 39 (2014) 1664–1667.
[75] Q. Meng, Z. Wang, Y. Shen, B. Yan, S. Wang, X. Ma, RSC Adv. 2 (2012) 8752–8761.
[76] R.Y. Wang, Z. Li, Chin. J. Catal. 35 (2014) 134–139.
[77] Y. Sato, T. Yamamoto, Y. Souma, Catal. Lett. 65 (2000) 123–126.
[78] Z.P. Du, L.H. Xiong, Z.K. Lin, X.L. Li, Y.G. Ding, Y.X. Wu, Chin. J. Chem. Eng. 22 (2014) 1117–1121.
[79] J. Ren, W. Wang, D.L. Wang, Z.J. Zuo, J.Y. Lin, Z. Li, Appl. Catal. A: Gen. 472 (2014) 47–52.